THE JOURNAL OF PHYSICAL CHEMISTRY C

Article

pubs.acs.org/JPCC

Transport of Vanadium and Oxovanadium Ions Across Zeolite Membranes: A Molecular Dynamics Study

Kevin R. Hinkle,[†] Cynthia J. Jameson,[‡] and Sohail Murad*[,†,§]

Departments of [†]Chemical Engineering and [‡]Chemistry, University of Illinois at Chicago, Chicago, Illinois 60607, United States

ABSTRACT: Redox flow batteries (RFBs) have become an attractive form of energy storage because of their safety, capacity, and small environmental footprint; however, this technology is not yet widely available due to inefficiencies in the ion-exchange membrane. The current technology widely utilizes polymeric membranes that have stability problems in the highly reactive environment of the RFB and tend to break down, shortening the life of the battery. Also, they present less than desirable selectivity for proton transport, which is crucial to the overall efficiency of the battery. It has been proposed that thin zeolite membranes will provide both the stability and the selectivity to improve the performance of RFBs and make their wide-scale application more feasible. A molecular dynamics study of six types of these membranes (ERI, LTA, MFI, BEC, CFI, DON) and the ions present in the vanadium-RFB has been undertaken to determine their transport behavior and investigate the molecular level requirements for their suitability for IEM applications. The hydration of the vanadium(II) [V^{2+}], vanadium(III) [V^{3+}], oxovanadium(IV) [VO^{2+}], and dioxovanadium(V) [VO_2^+] ions plays a key part in ion transport and was examined in detail. Structures and dynamics of the hydration shells were investigated and found to agree with previously reported findings when available. Ion transport was observed with the BEC, CFI, and DON zeolite framework types and the dynamics/properties of this transport were studied. It was found that a relatively large pore (~7 Å) was necessary for ion transport due to the strongly bound hydration shell that effectively increases the size of the ion. As the ions pass through the membrane, the shape and structure of their hydration shells remain unchanged. This verifies that the size of the hydrated ion complex is a key factor in zeolite membrane transport. The only ion transport observed through membranes with smaller pores (<5 Å) such as ERI, LTA, and MFI zeolite frameworks was that of the hydronium ion. Therefore, these membranes demonstrate the selective transport of hydronium ions over vanadium ions that is an essential requirement for IEMs in vanadium RFBs.

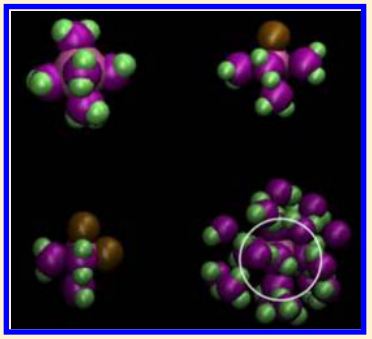

INTRODUCTION

As more effort is directed toward the generation of renewable or green energy, the need for a cost-effective and efficient means of storing that energy becomes an important issue that must be addressed. Methods of generation such as solar and wind power have shown the ability to produce electricity that exceeds immediate needs, which must then be stored for later use. To address this issue, redox flow batteries (RFBs) have been identified as a potential solution[1,2] due to their safety, high capacity, efficiency, and small environmental footprint. RFBs operate by converting electrical energy to chemical energy that is stored in reduced and oxidized ionic species (charging); this stored energy can then be converted back to electrical energy via electrochemical reactions and harnessed for use (discharging). The general principle of battery operation and a depiction of a functioning RFB operating within the renewable power system are shown in Figure 1.

To create an RFB with high storage capacity and high conversion efficiency, a number of conditions are necessary: the electrode reactions (shown below) must be reversible, both the oxidized and the reduced species must have a high solubility in the electrolyte solution, and there must be a large difference between the redox potentials. Several ion pairs have shown success in RFBs, including Fe/Cr,[3] Zn/Br,[4] and Zn/Ce.[5] The work here will focus on the well-known all-vanadium RFB.[6]

$$\text{cathode:}\quad VO^{2+} + H_2O - e^- \leftrightarrow VO_2^+ + 2H^+$$

$$\text{anode:}\quad V^{3+} + e^- \leftrightarrow V^{2+}$$

During charging or discharging operations, electrons flow through an external circuit, while protons remain internal and transport across an ion-exchange membrane (IEM) between the two electrode compartments. The IEM plays an important role in determining the efficiency and lifetime of an RFB.[7] It must be electrically insulating and impermeable to the reactive, vanadium species. Currently, most research and development has tended toward ion-exchange polymers, specifically sulfonated fluoropolymer copolymers (commercially known as Nafion).[8] These polymer membranes have demonstrated good stability and proton conductivity that lend themselves to applications in proton exchange membrane fuel cells (PEMFC) and direct methanol fuel cells (DMFC).[9] However, in RFBs, these membranes encounter two extreme operating conditions not present in PEMFCs or DMFCs. First, the polymeric membranes have low proton selectivity over multivalent cations. This leads to the crossover of reactive

Received: July 17, 2014
Revised: September 18, 2014
Published: September 23, 2014

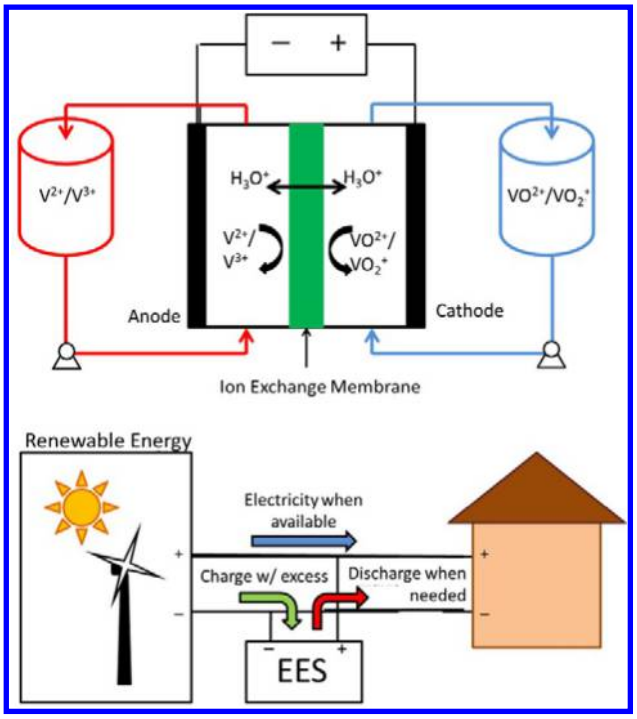

Figure 1. (Top) Principle of RFB operation. (Bottom) Schematic of RFB role within renewable power supply system.

ions and reduces the cell efficiency and lifetime of the electrolyte solutions.[8,10] Second, the highly oxidizing species present in RFBs tend to degrade the polymer membrane under the acidic and high-temperature operating conditions.[11,12] While improvements over the past few years have been made by modifying the polymeric membrane to increase selectivity and stability,[8] these limitations still inhibit the use of RFBs due to prohibitive cost and frequent maintenance necessary after electrolytic corrosion and ion crossover. Research on new materials that could act as an IEM must be undertaken if RFBs are to become a viable means of energy storage. This work focuses on using zeolite membranes as opposed to polymeric membranes. Zeolites are aluminosilicate crystals with ordered pore sizes varying from 0.3 to >1.0 nm, depending on the framework type. Zeolites with high Si/Al ratios are electrically insulating and are extremely stable in both acidic and basic conditions.[13−15] Previously, thin zeolite membranes have been used to confirm water/ion separation via the size-exclusion mechanism.[16−18] It is predicted that thin film zeolite membranes could be used as a superior class of IEMs in RFBs by addressing the issues of current polymeric membranes. In order to demonstrate the feasibility of the zeolite IEMs, they must prove to be selectively permeable to proton transport and not the cations present in the vanadium RFB, namely, the vanadium(II) ion (V^{2+}), the vanadium(III) ion (V^{3+}), the oxovanadium(IV), or vanadyl ion (VO^{2+}), and the dioxovanadium(V) or pervanadyl ion (VO_2^+). This selective permeability will be examined using the molecular dynamics technique to study the solvation of these vanadium-containing ions and the transport of water and ions through zeolite membranes with various pore sizes.

METHODS

Model Setup. This molecular dynamics study of transmembrane transport utilizes a system setup developed in previous work on osmosis/reverse osmosis and ion-exchange membranes;[16] it will therefore only be briefly discussed here. As seen in Figure 2, two membranes are used along with periodic

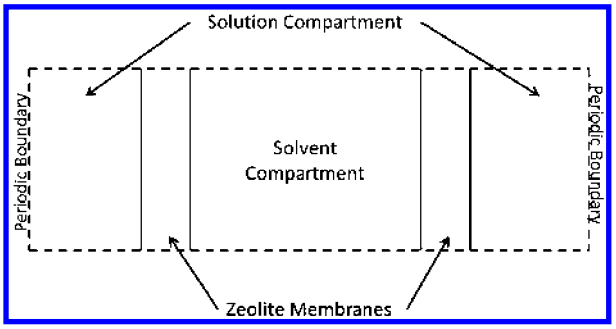

Figure 2. System schematic showing alternating solution/solvent compartments.

boundary conditions to create alternating solution/solvent compartments in the x-direction, while the system is infinite in the transverse dimensions (y,z)

In order to study the transport of the vanadium ions through porous media, six different zeolite structures were investigated. These were obtained from the IZA-SC's Database of Zeolite Structures (DZS).[19] The membranes used in our simulations were constructed as free-standing crystals with a thickness of one unit cell. Additionally, the framework consisted only of silicon and oxygen atoms. This differs from zeolite membranes used in experimental RFBs which are usually grown onto a porous substrate and can have thicknesses of several micrometers and Si/Al framework ratios around 4.[20] Even though the differences between the two are significant, single-cell thick model zeolite membranes have previously been shown to correctly reproduce experimental results of gas separation.[21] The length of the channel has no significant bearing on the selectivity of the membrane, only the transport rate. Selectivity occurs mainly at the entrance to the pore; if an ion can pass through here, cross-membrane transport should be observable at any channel length given a long enough time scale. Details such as pore sizes and total number of atoms in the system can be seen in Table 1. The number of atoms differs because the transverse dimensions of the zeolite frameworks are not uniform and the number of atoms in the solvent/solution compartments must be adjusted accordingly to ensure they exist at the desired densities. The center compartment initially consisted solely of water and the outer compartment contained aqueous solutions of the various cations and chloride ions (Cl^-) for charge balance. Atom counts for ions are not shown

Table 1. Zeolite Frameworks, Pore Sizes, and Total Atom Counts

membrane type	pore size[a] (Å)	atom count
DON	8.07	1560 membrane, 6100 H_2O
CFI	7.26	1476 membrane, 7475 H_2O
BEC	6.23	1980 membrane, 5065 H_2O
MFI	4.70	2736 membrane, 5380 H_2O
LTA	4.21	1584 membrane, 4343 H_2O
ERI	3.42	2064 membrane, 4510 H_2O

[a]Maximum diameter of a sphere that can diffuse through channel given that O-atoms have a radius of 1 Å.

dx.doi.org/10.1021/jp507155s | J. Phys. Chem. C 2014, 118, 23803−23810

in Table 1. These vary; numbers correspond to concentrations in the range 1−8 mol %.

The membrane atoms are tethered to their known equilibrium positions using a simple harmonic tether. Short-range site−site interaction potentials used the Lennard-Jones (LJ) and Coulombic models and are of the form:

$$U_{ij} = 4\varepsilon_{ij}\left[\left(\frac{\sigma_{ij}}{r_{ij}}\right)^{12} - \left(\frac{\sigma_{ij}}{r_{ij}}\right)^{6}\right] + C\frac{q_i q_j}{r_{ij}};\quad r_{ij} < r_c \tag{1}$$

where r_{ij} is the distance between sites i and j, r_c is the cutoff radius beyond which the short-range interactions are neglected, σ_{ij} and ε_{ij} are the LJ parameters, q_i and q_j represent the charges on sites i and j, and C is a unit conversion constant. These potentials are summed over all sites to obtain the total intermolecular interactions. Because the objective of this project was to obtain qualitative information about vanadium ion transport, previously developed parameters for water, ions, and zeolite membranes were used and can be seen in Tables 2 and 3. The water was modeled using the simple point charge (SPC) model,[22] while the zeolite was modeled with parameters from Lee et al.[23] The parameters for the various vanadium ions were taken from previous studies[24−26] as was the model for the hydronium ion.[27] Lorenz-Berthelot mixing rules were used for cross interactions between different sites. Harmonic potentials were also used to model intramolecular bonds and angles.

Table 2. Lennard-Jones Parameters and Charges

atom	σ (Å)	ε (kcal/mol)	q
Membrane			
Si	4.009	0.1275	0.0
O	2.89	0.1550	0.0
Water			
O	3.17	0.1554	−0.82
H	0.0	0.0	0.41
Ions			
V^{2+}/V^{3+}	2.432	0.0179	2.0/3.0
VO^{2+}/VO_2^{+}			
V	2.432	0.0179	2.7/2.0
O	3.17	0.1554	−0.7/-0.5
H_3O^{+}			
O	2.901	0.2741	−0.248
H	0.0	0.0	0.416
Cl^{1-}	4.33	0.1063	−1.0

Table 3. Bond Lengths and Angles

bond type	length (Å)	angle type	degree
O−H (water)	1.0	H−O−H (water)	109.47
O−H (H_3O^{+})	0.973	H−O−H (H_3O^{+})	111.6
V−O (VO^{2+}/VO_2^{+})	1.6	O−V−O (VO_2^{+})	105.0

Simulation Details. Initial configurations were created using a combination of Jmol[28] (to construct the zeolite crystal framework from CIF files provided by the DZS) and Packmol[29] (to construct nonoverlapping random solvent/solution initial configurations). All simulations were run using the LAMMPS simulation package.[30] Energy minimization was carried out using the Polak-Ribiere conjugate gradient method and the Verlet algorithm was used to perform time integration. The particle−particle/particle−mesh (PPPM) technique was used in the treatment of long-range Coulombic interactions beyond the cutoff radius of 1.2 nm. A Gaussian thermostat was applied to the NVE ensemble so that the system could maintain a constant temperature throughout the simulation. Except for the variable temperature studies, all simulations were carried out at 325 K, which is a typical operating temperature of vanadium RFBs. A time step of 0.5 fs was used for runs up to 5 ns in length (10 million steps).

RESULTS AND DISCUSSION

Hydration Shell Structure and Dynamics. Hydration studies were carried out in the bulk solution for ion concentrations of 1 mol%. The radial distribution function (Figure 3a) shows the peak of the first hydration shell of the vanadium(II) ion is at 2.1 Å and contains 6 water molecules while the peak of the first hydration shell of the oxovanadium-(IV) ion is smaller at 2.0 Å and only contains 5 water molecules while the dioxovanadium(V) shell is seen to only contain 4 water molecules. This systematic reduction in the hydration number occurs because the oxygen atoms in the oxovanadium-(IV) and dioxovanadium(V) ions effectively replace hydrating water molecules. Our V−O(H_2O) distances (2.0−2.1 Å) agree with both the previous quantum calculations of hydrated

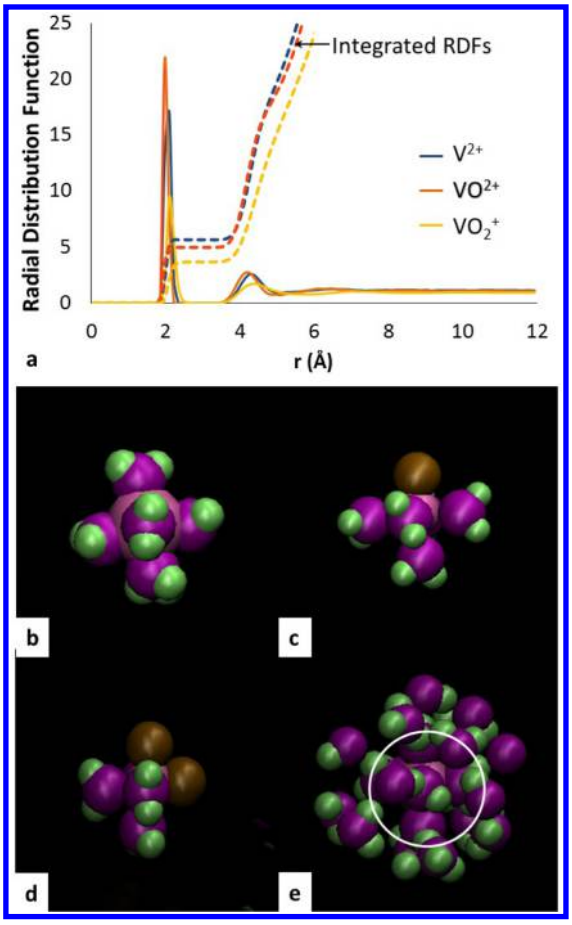

Figure 3. (a) Radial distribution function for V-O in V^{2+}-water, VO^{2+}-water, and VO_2^{+}-water; structures of first hydration shells of (b) vanadium(II), (c) oxovanadium(IV), and (d) dioxovanadium(V) ions. (e) Second hydration shell of vanadium(II) ion; circle approximates outer edge of first shell.

dx.doi.org/10.1021/jp507155s | J. Phys. Chem. C 2014, 118, 23803−23810

vanadium ions (2.17 Å)[31] and the experimentally measured octahedral structures of hydrated vanadium and oxovanadium/dioxovanadium ions obtained using EXAFS/LAXS (1.97−2.2 Å)[32] and NMR (2.2 Å)[33] techniques. Typical first hydration shells can be observed in Figure 3b. The second hydration shell also appears to be well defined for all four ions, and the case of V^{2+} is shown in Figure 3c. Similar analysis was performed on the vanadium(III) ion and its structure and RDF was found to be identical to that of the vanadium(II) ion. An interesting observation is that the entire first hydration shell lies within the Lennard-Jones size parameter, $\sigma_{V\text{-}O}$ (~2.1 vs 2.8 Å). This is due to the strong Coulombic interactions of the multivalent cations with SPC water.

The section after the first peak of the RDF for all three vanadium ion species has a value of zero, suggesting that there is a negligible exchange of water from the first hydration shell due to the high charge density of the vanadium ion. The octahedral shape is demonstrated by constructing a histogram of all the water−vanadium−water angles present during the simulation (Figure 4). The peaks at ~90° and ~180° in Figure 4a display the ordered structure of the shell and agree with QM/MM calculations performed by Loeffler et al.[31] The peak around 90° shifts to smaller angles as the oxidation state of the atom increases because as oxygen atoms replace water molecules in the hydration cluster, they push the remaining water away due to steric effects. In the case of the $[VO(H_2O)_5]^{2+}$ cluster, this means that the four "equatorial" waters are pushed out of plane with the vanadium atom, decreasing the angles between themselves and the remaining "pole" water. Likewise, in the $[VO_2(H_2O)_4]^{+}$ cluster, the presence of the two oxygen atoms causes the octahedral structure to skew further as the four remaining water molecules shift toward one another to make room for the covalently bonded O-atom. These structures agree with X-ray scattering measurements made by Krakowiak et al.[32] Compare these regular structures to the broad distribution of angles found in the chloride hydration shell (Figure 4b), which indicates a much more fluid, looser hydration structure with considerable exchange between water in the first and second hydration shells.

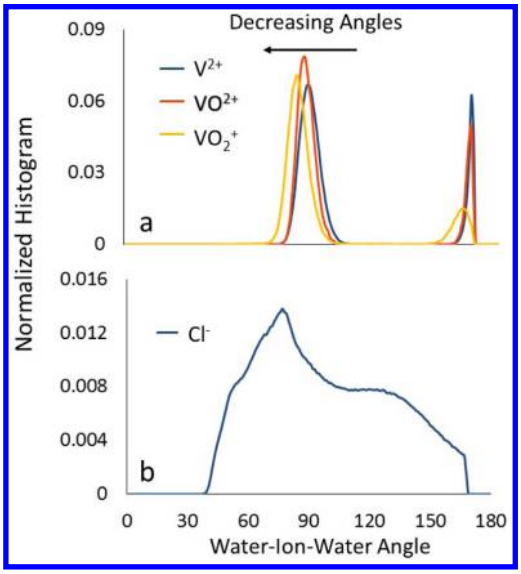

Figure 4. Angular distribution showing occurrences of (a) water−V−water angles for vanadium(II), oxovanadium(IV), and dioxovanadium-(V) and (b) water−Cl−water angles for chloride ions in aqueous solution.

The same structural angle analysis is performed when the ions are both confined within the different membrane types and within an "entrance region" defined as ±1 Å from the membrane surface (Figure 5). Comparison of the graphs in Figures 4a with Figure 5a,b demonstrates that the shape of the $[V(H_2O)_6]^{2+}$ cluster does not change as it moves out of the solution compartment, through the entrance region, and into the center of the membrane. Similar results were observed for the $[VO(H_2O)_5]^{2+}$ and $[VO_2(H_2O)_4]^{+}$ clusters. This further supports the idea of a rigid structure for these ions. In contrast, the deformation of the Cl^- hydration shell as it passes through the smaller pore of the BEC membrane is evident as a result of its less rigid structure (due to lower surface charge density) in Figure 5c. The statistically noisier histograms in Figure 5 compared to Figure 4 arise from the fewer observations of ions at these specific regions in comparison to the bulk solution.

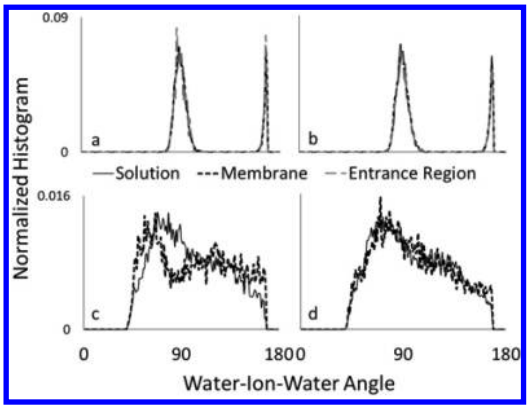

Figure 5. Histograms of water−ion−water angles present during cross-membrane transport: (a) V^{2+}/BEC, (b) V^{2+}/DON, (c) Cl^-/BEC, (d) Cl^-/DON.

The residence time of waters within the hydration shell in bulk solution was measured using the method of Impey et al.,[34] which expresses the residence time as

$$\tau_{res} = \int_0^\infty R(t)\mathrm{d}t \tag{2}$$

where $R(t)$ is a residence time correlation function defined as

$$R(t) = \frac{1}{N_h}\sum_{i=1}^{N_h}\langle\theta_i(t)\theta_i(0)\rangle \tag{3}$$

where N_h is the number of hydrating water molecules and $\theta_i(t)$ is a Heaviside step function that equals 1 if the ith hydrating water molecule is in the hydration shell at time t and equals zero in all other instances. Water exchange from the vanadium hydration shell was not observed during our simulation time of 5 ns. This is not surprising as experimental values obtained via NMR and reported for other bivalent metal cations by Ohtaki and Radnai[35] are on the order of 32 to 200 ns, which demonstrates that a longer time scale would be necessary to observe this phenomena, which again confirms the presence of a relatively stable complex. On the other hand, a residence time of ~11 ps was observed for the chloride ion, which agrees with values of previous simulation studies[36] and indicates a much

dx.doi.org/10.1021/jp507155s | J. Phys. Chem. C 2014, 118, 23803−23810

Table 4. Solvation Energy of 1 mol% V^{2+}, V^{3+}, VO^{2+}, VO_2^+, and Cl^- at 325 K

ion	this work (kcal/mol·Å)	experimental values[a] (kcal/mol·Å)	% difference	previous calculation results[b] (kcal/mol·Å)	% difference
V^{2+}	−401.8 ± 3.2	−436.2	7.9	−440.0	8.7
V^{3+}	−800.5 ± 4.1	−1008.6	20.6	−1018.8	21.4
VO^{2+}	−421.3 ± 3.1	[c]	[c]	−457.2	7.9
VO_2^+	−177.2 ± 2.0	[c]	[c]	−184.4	3.9
Cl^-	−89.3 ± 1.6	−86.4	3.4	−89.2	0.1

[a]See Marcus.[38] [b]See Sepehr et al.[37] and Smith et al.[39] [c]We are not aware of experimental data for these multiatomic cations.

more dynamic, unstructured hydration shell that is dramatically shown in Figure 4 to be in stark contrast to the vanadium ions.

Solvation Energy Analysis. Solvation energy is defined as the energy released as the isolated ion associates with solvent molecules. The solvation energy of an ion was obtained by calculating the pairwise potential energy between the ion and all other atoms within a 1.2 nm radius in the bulk solution. This was done for ion concentrations of 1 mol%, which is close to working concentrations of experimental RFBs (~0.6 mol%).[6] Here the values are time averaged over the last nanosecond of the simulation and error range represents ± 1σ. Our results (Table 4) agree with calculations based on a first principles model that used quantum electronic structure calculations.[37] We propose that the relatively larger error in our value for vanadium(III) can be explained by polarization of surrounding water molecules due to the extremely high charge density of the V^{3+} ion. The SPC water model does not account for this phenomenon, whereas the quantum calculation does. This difference is not predicted to have a large impact on the transport behavior of the vanadium(III) ion because our model still correctly represents the physical structure of the $[V(H_2O)_6]^{3+}$ cluster. The close agreement for all other ions shows that our model well represents their aqueous behavior and should therefore produce realistic transport results.

Transport Analysis. In order to better understand the transport of the hydrated ions through the various zeolite pores, a single ion was placed on the pore axis and passed through the membrane at a constant velocity of 0.75 m/s. This steered molecular dynamics (SMD) technique allows for the calculation of the Kirkwood potential of mean force (PMF)[40] for the transport of a single hydrated ion across the membrane. The PMF is defined as the potential that yields the average force for all configurations along the "reaction path". This calculation was performed in the same manner as previous studies.[41] First, the force required to keep the hydrated ion on the pore axis is considered to be the opposite of the total pairwise force on the ion and is found using the following equation:

$$F_c = -F_p = \nabla U \tag{4}$$

where U is the potential defined in eq 1. This force is then integrated with respect to the path maintained by the SMD, which in this case is one-dimensional along the axis of the pore:

$$\mathrm{PMF} = \int F_c \cdot \mathrm{d}r = \int F_{cx} \mathrm{d}x \tag{5}$$

The profiles obtained represent the free energy barriers that must be overcome for the transport of ions to occur and are shown in Figure 6. All graphs in Figure 6 are drawn at the same scale in order to provide direct visual comparison.

The jagged nature of the PMF for the ERI membrane is due to the changing number of water molecules in the hydration shell as it moves through the membrane. These pores are small

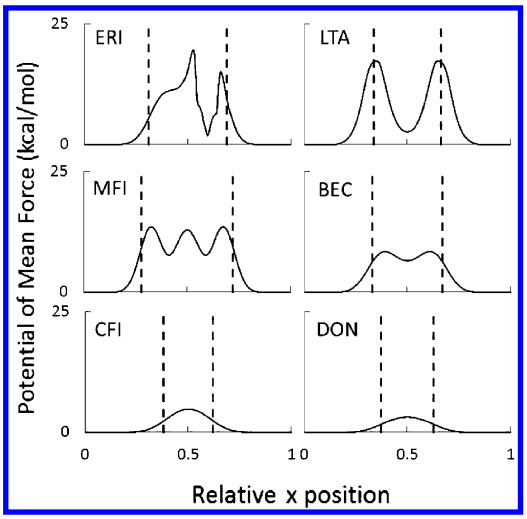

Figure 6. Potentials of mean force for hydrated V^{2+} ion passing through the six membrane framework types at 325 K.

enough that in order for the ion to be forced through, it must shed some of the hydrating waters so that the cluster is not as large. On exiting the membrane, the ion is hydrated again resulting in the reappearance of the stable cluster. The ERI profile also appears to be asymmetric. This is due to the rather rapid motion of the ion through the membrane (0.75 m/s), which does not allow enough time for the changing number of water molecules in the hydration shell to approach "local equilibrium". The LTA, MFI, and BEC membranes display local minima where the presence of a hydrated ion complex is most favorable. These minima correspond to a cavity at the intersection of the channels running in three directions within the zeolite membrane. The only maximum for the CFI and DON membranes is at the center because their pores are one-dimensional channels. In Figure 7, it can be seen that the free energy barrier decreases with increasing pore size. The same analysis was conducted using the other vanadium ions and their

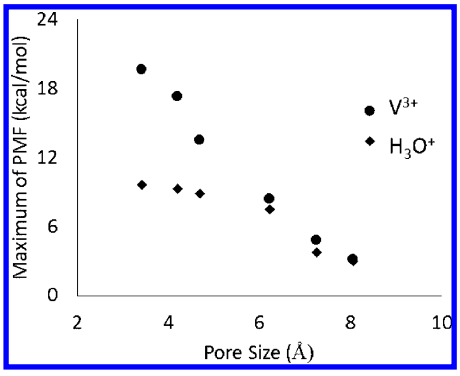

Figure 7. Values of free energy barriers for different ions.

dx.doi.org/10.1021/jp507155s | J. Phys. Chem. C 2014, 118, 23803−23810

PMF profiles were nearly identical to that for V^{2+}. On the other hand, the hydronium ion profiles are quite different from the vanadium ions. A comparison of PMF peak values is shown between V^{3+} and H_3O^+ ions in the six zeolites in Figure 7. The marked differences in the free energy barriers for the vanadium ions and hydronium ions for zeolites with pores <5Å is indicative of the selective transport that we seek in effective IEMs.

Because the $[V(H_2O)_6]^{2+/3+}$, $[VO(H_2O)_5]^{2+}$, and $[VO_2(H_2O)_4]^+$ complexes have such stable octahedral structures, we can also investigate any changes in orientation of the hydrated ions as they traverse the membrane during our steered simulations. This was done by observing the angle between: (1) a single $V^{2+/3+}$−water pair and the pore axis in the case of $V^{2+/3+}$, (2) the V−O bond and the pore axis in the case of VO^{2+}, and (3) a single V−O bond and the pore axis in the case of VO_2^+; this analysis is shown in Figure 8.

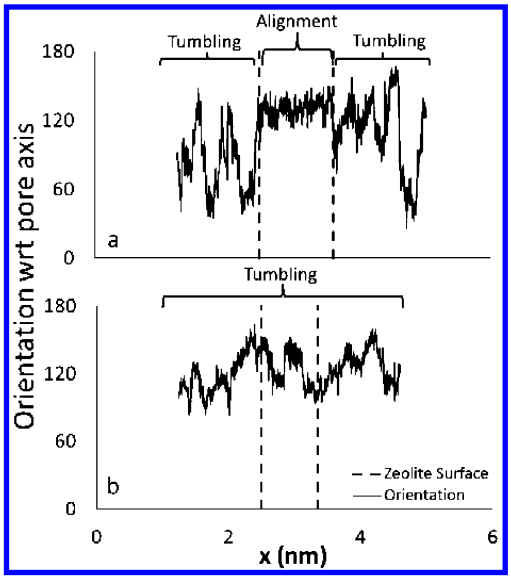

Figure 8. Orientation of the $[V(H_2O)_6]^{2+}$ complex during membrane transport in (a) BEC and (b) DON zeolite membrane.

Outside the membrane the $[V(H_2O)_6]^{2+}$ complex tumbles in random fashion. In the smaller pore of the BEC membrane (Figure 8a) the complex is seen to assume a particular orientation in the laboratory frame and remain in that orientation while in the channel. This orientation is the only one that permits the cluster to fit through the BEC pore because of their nearly identical dimensions (~6.08 Å for the cluster and ~6.23 Å for the pore). On the other hand, while passing through the larger pore of the DON membrane (Figure 8b), the complex randomly tumbles along the entire path. This contrast in behavior of the $[V(H_2O)_6]^{2+}$ complex again indicates the higher free energy barrier that must be overcome for the V^{2+} ion to pass through the BEC membrane compared to the DON. We have seen that this barrier is even greater in those membranes with even smaller pores.

The previous studies examined a single ion being steered through the zeolite pore systems. Systems at higher ion concentrations were also studied in this work and the amount of ions that crossed the membrane spontaneously was measured. In order to ensure the observation of transport events, both the ion concentration and the temperature were increased to values above those of operating RFBs (8 mol%, 400 K). In these MD simulations, it is notable that even at these extreme conditions, the only transport observed through the ERI, LTA, and MFI membranes was that of the hydronium ions. These three membrane frameworks blocked the transport of all vanadium ions (Figure 9a). Therefore, these membranes

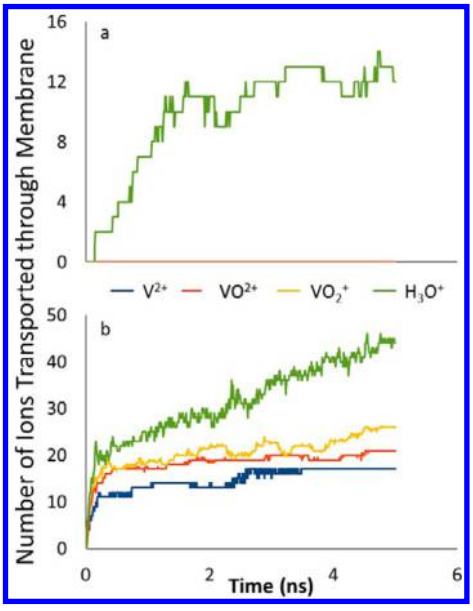

Figure 9. Ion transport events for (a) MFI framework (straight channel) and (b) DON framework at 8 mol % and 400 K.

demonstrate the selectivity necessary for successful application toward efficient RFBs. This result agrees with selective transport observed experimentally by Xu et al.[20] while using substrate-supported zeolite membranes containing the ERI framework. On the other hand, the larger pores in the BEC, CFI, and DON frameworks allowed for the transport of all ion species V^{2+}, V^{3+}, VO^{2+}, and VO_2^+ in addition to hydronium ions (Figure 9b), which would be unacceptable for an ion-exchange membrane in the vanadium redox flow battery.

Significant vanadium-ion transport through the membrane did not occur until the pore size had reached 7.26 and 8.07 Å in the CFI and DON zeolite frameworks. At these pore sizes the ions freely traversed the membrane, entered the center compartment, and dispersed; but this occurred only when the solution compartment was at concentrations higher than 5 mol % for the CFI pore and 3 mol % for the DON pore. This suggests that there exists both a critical pore size and a critical ion concentration for the observation of ion transport. Higher ion concentrations predictably increased the transport of ions, while higher temperatures increased the initial rate of transport. These trends are shown in Figure 10 for the DON membrane, but they also present themselves in the case of the CFI framework.

Similar runs examining the oxovanadium(IV) and dioxovanadium(V) ions presented identical trends as that shown in Figure 10 for V^{2+} in DON. However, the degree of transport increased with the oxidation state of the vanadium atom in the order $VO_2^+ > VO^{2+} > V^{2+}$. This is attributed to the effective size of the hydration cluster; the covalently bonded oxygen atoms are closer to the vanadium center (~1.6 Å) than are the hydrating water molecules (~2.1 Å). In order to further study this spontaneous membrane transport in the DON

dx.doi.org/10.1021/jp507155s | J. Phys. Chem. C 2014, 118, 23803−23810

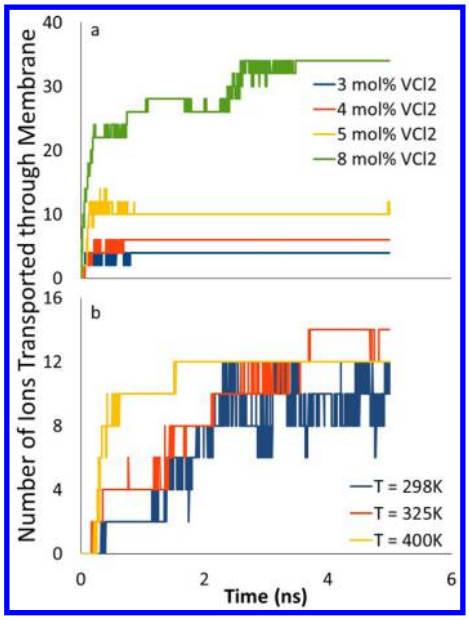

Figure 10. Dependence of V^{2+} ion transport for the DON zeolite membrane on (a) ion concentration and (b) temperature.

zeolite membrane, profiles of average velocity and residence time of V^{2+} ions are shown in Figure 11.

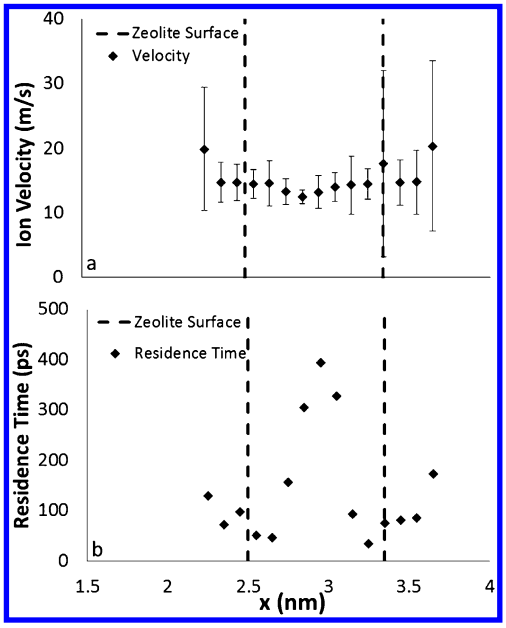

Figure 11. Profiles of (a) velocity and (b) residence time of V^{2+} ions within the DON membrane for 8 mol% solution at 400 K.

It is observed that velocities of ions outside the DON membrane are higher and have more variation than the velocities inside (Figure 11a). While it may appear that the ion velocity slows at the center of the membrane, this cannot be determined with certainty as the ion maintains a constant velocity within 1 standard deviation as it crosses the membrane. There is, however, an increase in the residence time at the center of the membrane (Figure 11b). This residence time was defined as the average amount of time spent in a volume element 0.1 Å wide in the *x*-direction before moving to an adjacent volume element. This significantly higher residence time in the center also indicates that there is significant motion in the *y*/*z*-directions as well at the center of the membrane (Figure 11a includes velocities in all three directions, while in Figure 11b we measure transport in the *x*-direction only). On average, the V^{2+} ions spend anywhere between 50 and 3000 ps within the DON membrane, with 67% of crossing ions spending less than 200 ps. These residence times are only ∼4% of our simulation time, which suggests that, while the hydrated V^{2+} ions can freely transport through the pores of the DON zeolite at this temperature, because the temperature is less than ∼1600 K, which is $(1/k_B)$ times the barrier height in this case, it is more favorable for the hydrated ion clusters to be present in bulk solution outside the membrane where they can be fully solvated.

■ CONCLUSIONS

Our work has reproduced observed hydration structures and ab initio calculated hydration energies for the vanadium(II), vanadium(III), oxovanadium(IV), and dioxovanadium(V) ions. Examination of both the structure and the dynamics of these clusters during membrane transport yields a number of observations. The octahedral structure of the hydration shells is very rigid, and no deformation occurs, even when in close proximity to the pore walls. This rigid structure requires a larger pore in order for membrane transport to occur, and when it does, the clusters spend short periods of time actually present inside the pores. Based on the practical requirement that IEMs in RFBs be impermeable to the electrochemically reactive ions, a framework type with a small enough pore must be selected while still allowing for the transport of water and hydronium ions. The three membranes with larger pores examined in this study (DON, CFI, BEC) would not be suitable for use in a vanadium-RFB; in the case of the DON and CFI frameworks, the facile transport of vanadium containing ions would greatly reduce the efficiency and lifetime of the battery. The BEC framework allowed vanadium containing ions to enter the pores, which would reduce efficiency. The three membranes with smaller pores (MFI, LTA, ERI) were shown to block all vanadium transport at the conditions present in this study while still allowing for the hydronium transport required for the operation of RFBs. Therefore, these zeolite types are recommended as feasible IEM materials. The more practical zeolite forms to use are those with some Al replacing Si in the framework, for example, a Si/Al ratio of ∼4, as these are known to be more stable to acids and high temperatures. Our conclusions based on all-Si zeolites apply, since the framework structure itself remains essentially unchanged with this extent of Al substitution. This classical MD simulation only considered the diffusion of protonated water molecules. There exists an additional mechanism for proton transport in zeolite IEMs which involves the "hopping" along sequences of water molecules (Grothuss diffusion). The latter requires a quantum description of proton movement from a hydronium ion to a neighboring water molecule and is therefore beyond the scope of the present study. Finally, our conclusions are based on thin membranes constructed of single crystal structures in our simulations, while actual zeolite membranes, as synthesized, may involve crystal intergrowths, defects, and other imperfections that may result in nonuniform channels, nonuniform axis orientations, or even incomplete walls. It is obviously necessary to fully characterize the as-synthesized membrane structure before attempting to use it for IEM purposes.

dx.doi.org/10.1021/jp507155s | J. Phys. Chem. C 2014, 118, 23803−23810

AUTHOR INFORMATION

Corresponding Author

*E-mail: smurad1@iit.edu

Present Address

[§]Department of Chemical and Biological Engineering, Illinois Institute of Technology, Chicago, IL 60616, United States (S.M.).

Notes

The authors declare no competing financial interest.

ACKNOWLEDGMENTS

This work has been supported by a grant from the National Science Foundation (Grant No. CBET-1263707).

REFERENCES

(1) Ponce de Léon, C.; Frías-Ferrer, A.; González-García, J.; Szánto, D. A.; Walsh, F. C. Redox Flow Cells for Energy Conversion. *J. Power Sources* **2006**, *160*, 716−730.

(2) Cheng, F.; Liang, J.; Tao, Z.; Chen, J. Functional Materials for Rechargeable Batteries. *Adv. Mater.* **2011**, *23*, 1695−1715.

(3) Codina, G.; Perez, J. R.; Lopez-Atalaya, M.; Vazquez, J. L.; Aldaz, A. Development of a 0.1 kW Power Accumulation Pilot-Plant Based on an FE/CR Redox Flow Battery Part I. Consideration on Flow-Distribution Design. *J. Power Sources* **1994**, *48*, 293−302.

(4) Lim, H. S.; Lackner, A. M.; Knechtli, R. C. Zinc-Bromine Secondary Battery. *J. Electrochem. Soc.* **1977**, *124*, 1154−1157.

(5) Clarke, R. L.; Dougherty, B. J.; Harrison, S.; Millington, J. P. Battery with Bifunctional Electrolyte. U.S. Patent Application, International Publication No. 1932-7447, 2004.

(6) Skyllas-Kazacos, M.; Rychcik, M.; Robins, R. G.; Fane, A. G.; Green, M. A. New All-Vanadium Redox Flow Cell. *J. Electrochem. Soc.* **1986**, *133*, 1057.

(7) Díaz-González, F.; Sumper, A.; Gomis-Bellmunt, O.; Villafáfila-Robles, R. A Review of Energy Storage Technologies for Wind Power Applications. *Renew. Sustain. Energy Rev.* **2012**, *16*, 2154−2171.

(8) Li, X.; Zhang, H.; Mai, Z.; Zhang, H.; Vankelecom, I. Ion Exchange Membranes for Vanadium Redox Flow Battery (VRB) Applications. *Energy Environ. Sci.* **2011**, *4*, 1147−1160.

(9) Li, X. *Principles of Fuel Cells*; Talyor and Francis: New York, 2006.

(10) Vijayakumar, M.; Bhuvaneswari, M. S.; Nachimuthu, P.; Schwenzer, B.; Kim, S.; Yang, Z.; Liu, J.; Graff, G. L.; Thevuthasan, S.; Hu, J. Spectroscopic Investigations of the Fouling Process on Nafion Membranes in Vanadium Redox Flow Batteries. *J. Membr. Sci.* **2011**, *366*, 325−334.

(11) Mohammadi, T.; Skyllas-Kazacos, M. Evaluation of the Chemical Stability of Some Membranes in Vanadium Solution. *J. Appl. Electrochem.* **1997**, *27*, 153−160.

(12) Dai, H.; Zhang, H. M.; Zhong, H. X.; Li, X. F.; Xiao, S. H.; Mai, Z. S. High Performance Composite Membranes with Enhanced Dimensional Stability for Use in PEMFC. *Int. J. Hydrogen Energy* **2010**, *35*, 4209−4214.

(13) Lew, C. M.; Cai, R.; Yan, Y. S. Zeolite Thin Films: From Computer Chips to Space Stations. *Acc. Chem. Res.* **2010**, *43*, 210−219.

(14) Deng, S. G.; Lin, Y. S. Sulfur Dioxide Sorption Properties and Thermal Stability of Hydrophobic Zeolites. *Ind. Eng. Chem. Res.* **1995**, *34*, 4063−4070.

(15) *Handbook of Zeolite Science and Technology*; Auderbach, S. M., Carredo, K. A., Dutta, P. K., Eds.; Dekker: New York, 2003.

(16) Lin, J.; Murad, S. A Computer Simulation Study of the Separation of Aqueous Solution Using Thin Zeolite Membranes. *Mol. Phys.* **2001**, *99*, 1175−1181.

(17) Li, L.; Dong, J.; Nenoff, T. M.; Lee, R. Desalination by Reverse Osmosis Using MFI Zeolite Membranes. *J. Membr. Sci.* **2004**, *243*, 401−404.

(18) Li, L.; Dong, J.; Nenoff, T. M.; Lee, R. Reverse Osmosis of Ionic Aqueous Solutions on a MFI Zeolite Membrane. *Desalination* **2004**, *170*, 309−316.

(19) Baerlocher, Ch.; McCusker L. B.; Olson, D. H. *Atlas of Zeolite Framework Types*, 6th ed.; Elsevier Science: New York, 2007.

(20) Xu, Z.; Michos, I.; Wang, X.; Yang, R.; Gub, X.; Dong, J. A Zeolite Ion Exchange Membrane for Redox Flow Batteries. *Chem. Commun.* **2014**, *50*, 2416−2419.

(21) Jia, W; Murad, S. Separation of Gas Mixtures Using a Range of Zeolite Membranes: A Molecular-Dynamics Study. *J. Chem. Phys.* **2005**, *122*, 234708−234718.

(22) Berendsen, H. J. C.; Postma, J.; Gunsteren, W. F. In *Intermolecular Forces*; Pullman, B., Ed.; Reidel: Dordrecht, 1981.

(23) Lee, S. H.; Moon, G. K.; Choi, S. G.; Kim, H. S. Molecular Dynamics Simulation Studies of Zeolite-A. 3. Structure and Dynamics of Na^+ Ions and Water Molecules in a Rigid Zeolite-A. *J. Phys. Chem.* **1994**, *98*, 1561−1569.

(24) Li, P.; Roberts, B. P.; Chakravorty, D. K.; Merz, K. M. Rational Design of Particle Mesh Ewald Compatible Lennard-Jones Parameters for +2 Metal Cations in Explicit Solvent. *J. Chem. Theory Comput.* **2013**, *9*, 2733−2748.

(25) Evans, J. C. The Vibrational Spectra and Structure of the Vanadyl Ion in Aqueous Solution. *Inorg. Chem.* **1963**, *2*, 372−375.

(26) Persson, I. Hydrated Metal Ions in Aqueous Aolution: How Regular Are Their Structures? *Pure Appl. Chem.* **2010**, *82*, 1901−1917.

(27) Kusaka, I.; Wang, Z. G.; Seinfeld, J. H. Binary Nucleation of Sulfuric Acid−Water: Monte Carlo Simulation. *J. Chem. Phys.* **1998**, *108*, 6829−6848.

(28) Jmol: an open-source Java viewer for chemical structures in 3D; http://www.jmol.org/.

(29) Martínez, L.; Andrade, R.; Birgin, E. G.; Martínez, J. M. Packmol: A Package for Building Initial Configurations for Molecular Dynamics Simulations. *J. Comput. Chem.* **2009**, *30*, 2157−2164.

(30) Plimpton, S. Fast Parallel Algorithms for Short-Range Molecular Dynamics. *J. Comp. Phys.* **1995**, *117*, 1−19.

(31) Loeffler, H. H.; Yague, J. I.; Rode, B. M. QM/MM−MD Simulation of Hydrated Vanadium(II) Ion. *Chem. Phys. Lett.* **2002**, *363*, 367−371.

(32) Krakowiak, J.; Lundberg, D.; Persson, I. A Coordination Chemistry Study of Hydrated and Solvated Cationic Vanadium Ions in Oxidation States +III, +IV, and +V in Solution and Solid State. *Inorg. Chem.* **2012**, *51*, 9598−9609.

(33) Vijayakumar, M.; Burton, S. D.; Huang, C.; Li, L; Yang, Z; Graff, G. L.; Liu, J.; Hu, J.; Skyllas-Kazacos, M. Nuclear Magnetic Resonance Studies on Vanadium(IV) Electrolyte Solutions for Vanadium Redox Flow Battery. *J. Power Sources.* **2010**, *195*, 7709−7717.

(34) Impey, R. W.; Madden, P. A.; McDonald, I. R. Hydration and Mobility of Ions in Solution. *J. Phys. Chem.* **1983**, *87*, 5071−5083.

(35) Ohtaki, H.; Radnai, T. Structure and Dynamics of Hydrated Ions. *Chem. Rev.* **1993**, *93*, 1157−1204.

(36) Rasiah, J. C.; Lynden-Bell, R. M. Computer Simulation Studies of the Structure and Dynamics of Ions and Non-Polar Solutes in Water. *Philos. Trans. R. Soc., A* **2001**, *359*, 1545−1574.

(37) Sepehr, F.; Paddison, S. J. The Solvation Structure and Thermodynamics of Aqueous Vanadium Cations. *Chem. Phys. Lett.* **2013**, *585*, 53−58.

(38) Marcus, Y. Thermodynamics of Solvation of Ions. Part 5. Gibbs Free Energy of Hydration at 298.15 K. *J. Chem. Soc., Faraday Trans.* **1991**, *87*, 2995−2999.

(39) Smith, E. J.; Bryk, T.; Haymet, A. D. J. Free Energy Solvation of Simple Ions: Molecular-Dynamics Study of Solvation of Cl^- and Na^+ in the Ice/Water Interface. *J. Chem. Phys.* **2005**, *123*, 34706.

(40) Kirkwood, J. G. Statistical Mechanics of Fluid Mixtures. *J. Chem. Phys.* **1935**, *3*, 300−313.

(41) Song, B.; Yuan, H.; Jameson, C. J.; Murad, S. Role of Surface Ligands in Nanoparticle Permeation Through a Model Membrane: A Coarse-Grained Molecular Dynamics Simulations Study. *Mol. Phys.* **2012**, *110*, 2181−2195.